Journal of Materials Chemistry A

PAPER

View Article Online
View Journal | View Issue

Cite this: J. Mater. Chem. A, 2014, 2, 9875

Gold photosensitized $SrTiO_3$ for visible-light water oxidation induced by Au interband transitions†

Lequan Liu,[ab] Peng Li,[b] Boonchun Adisak,[be] Shuxin Ouyang,[bc] Naoto Umezawa,[bc] Jinhua Ye,*[abc] Rajesh Kodiyath,[b] Toyokazu Tanabe,[b] Gubbala V. Ramesh,[b] Shigenori Ueda[d] and Hideki Abe[bc]

Received 22nd April 2014
Accepted 27th April 2014

DOI: 10.1039/c4ta01988a

www.rsc.org/MaterialsA

Gold nanoparticle (NP) photosensitization over semiconductors with a large band gap has emerged as a promising strategy for developing visible-light responsive photocatalytic materials. However, its application in harsh photocatalytic oxidation still remains a significant challenge. Furthermore, energetic charge carriers created in Au interband transitions under visible light are frequently ignored in this field. In the current work, for the first time, a remarkable visible-light photocatalytic water oxidation activity (14.9 μmol h^{-1}: 0.2 g catalyst, 5 mmol $AgNO_3$), even slightly higher than that of commercial WO_3, was achieved over Au photosensitized $SrTiO_3$ (1.1 wt%). In an elaborate study, electron transfer from gold to $SrTiO_3$ was confirmed by STEM-EDS characterization on selective Ag deposition over $SrTiO_3$. A combined investigation of apparent quantum efficiency results, theoretical simulation study on Au NPs optical excitation and relative band position analysis in Au/$SrTiO_3$ reveals that these hot electrons transferred from gold to $SrTiO_3$ mainly come from Au interband transitions other than plasmon resonance, while leaving holes on Au with enough oxidative potentials are responsible for water oxidation. The capability of involving Au interband transition in photosensitization for visible light water oxidation opens up new opportunities in designing and preparing visible-light responsive photocatalysts.

Introduction

Harvesting abundant and renewable sunlight in chemical energy production and environmental remediation has attracted an enormous amount of research efforts, particularly in heterogeneous photocatalysis.[1] Various semiconductors with large band gaps have been proven to be effective under UV light, *e.g.*, TiO_2.[2] However, UV light accounts for only ~4% while visible light occupies ~43% of total sunlight. From the perspective of both chemistry and practical applications, it is undoubtedly important to develop photocatalytic materials that harvest a wide range of visible photons. Many strategies, including metal-ion and nonmetal doping,[3–5] have been proposed to extend absorption of semiconductors to the visible regions. However, to date, most of the doped materials have typically suffered from photocorrosion, thermal instability and fast e^-/h^+ recombination rates. Over the past several years, incorporating coinage metal nanoparticles (Au, Ag, Cu NPs) with visible-light absorption onto semiconductors has emerged as a promising new strategy for this issue.[6–9] Recently, we demonstrated that broadband visible-light harvesting over TiO_2 can be obtained by introducing Au nanorods as antennas.[10]

Coinage metal NP photosensitized semiconductors and pure plasmonic metals have been found to show visible-light responses in various applications such as dye degradation, organic pollutant removal, and fine chemical synthesis.[11,12] However, except for some findings in photoelectrocatalysis,[13–16] photosensitization of semiconductors with a large band gap (>3.1 eV) to achieve relatively harsh photocatalytic oxidation under visible light, *e.g.*, water oxidation, still remains a significant challenge.[17,18] This is understandable when taking into account the relatively high oxidative potential required for water oxidation ($2H_2O \rightarrow O_2 + 4H^+ + 4e$, 1.23 V *versus* NHE). On the other hand, water oxidation is the rate-determining step of pure water splitting and is also a critical step for the photoreduction of carbon dioxide with water to form hydrocarbons.[19,20] Therefore, much effort is required to address this reaction, in particular for developing visible-light responsive innovative candidates.

Valence electrons in metals can not only be excited to a collective oscillation state around Fermi level (E_F), known as

[a]International Center for Materials Nanoarchitectonics (WPI-MANA), 1-1 Namiki, Tsukuba, Ibaraki 305-0044, Japan. E-mail: jinhua.ye@nims.go.jp
[b]Environmental Remediation Materials Unit, National Institute for Materials Science (NIMS), 1-1 Namiki, Tsukuba, Ibaraki 305-0044, Japan
[c]TU-NIMS Joint Research Center, School of Material Science and Engineering, Tianjin University, 92 Weijin Road, Tianjin, P.R. China
[d]Synchrotron X-ray Station at SPring-8, NIMS, 1-1-1 Kouto, Sayo, Hyogo, 679-5148, Japan
[e]Department of Physics, Kasetsart University, Bangkok 10900, Thailand

† Electronic supplementary information (ESI) available. See DOI: 10.1039/c4ta01988a

localized surface plasmon resonance (LSPR), but can also be excited to an available conduction band above the E_F, which is referred to as an interband transition.[21] For gold, plasmon band overlaps and couples with interband transition in the visible light region.[22] Though the process that LSPR induced electron transfer from gold to semiconductors was frequently cited to explain the enhanced visible-light photocatalytic performance, energetic charge carriers created in interband transitions possessing higher redox potentials should be more favorable to drive harsh photocatalytic reactions. A few reports of photocatalytic oxidation on Au catalysts under UV light have been explained in the context of interband transition.[23–25] However, although some contributions hint at the possibility of involving interband transition,[26,27] to the best of our knowledge, there has been little fundamental evidence till now to correlate the visible-light activity of Au NP photosensitized photocatalysts to Au interband transition.

In the current study, for the first time, a remarkable visible light photocatalytic water oxidation activity, even slightly higher than that of the commercial WO_3, was achieved over Au NP photosensitized $SrTiO_3$. Moreover, direct electron transfer from gold to $SrTiO_3$ was confirmed by an STEM-EDS study on selective Ag deposition over $SrTiO_3$. A combination of apparent quantum efficiency results, theoretical simulation study on Au NPs optical excitation and relative band position analysis in Au/$SrTiO_3$ shows that these hot electrons transferred from gold to $SrTiO_3$ mainly come from Au interband transitions other than plasmon resonance, while the leaving holes on Au with enough oxidative potential are responsible for water oxidation.

Experimental section

Material preparation

$SrTiO_3$ nanoparticles were prepared with a modified PC method. The procedure and products are illustrated in Fig. S1.† In brief, 2.88 ml $Ti(OC_4H_9)_4$ (Wako, min. 95.0%) was dissolved in 10 ml 2-methoxyethanol, denoted as solution A. Then, 2.18 g $SrCl_2 \cdot 6H_2O$ (Wako, min. 99.0%) was dissolved in 10 ml 2-methoxyethanol, denoted as solution B, and 30 g citric acid (CA, Wako, min. 98.0%) was dissolved in 30 ml 2-methoxyethanol with heating, denoted as solution C. Solutions A and B were mixed and stirred for 0.5 h to obtain a sol, as shown in Fig. S1.† This sol was transmitted to solution C and continually stirred for 10 min. After that, 5 ml dehydrated ethylene glycol (EG, Wako, min. 99.5%) was added. The mixture was then heated to 125 °C at an increasing rate of 1 °C min^{-1} and maintained for 20 h to evaporate the 2-methoxyethanol solvent. Subsequently, polymerization was carried out at 130 °C for another 20 h. The obtained brown resin was cooled to room temperature. Finally, the resin was heated in a stove at 300 °C for 3 h and calcined at 500 °C for 5 h at an increasing rate of 1 °C min^{-1}. Organic frames were completely removed by calcination at 500 °C, as confirmed by TG-DTA plots (Fig. S2†). The resulting white powder was denoted as $SrTiO_3$. Commercial $SrTiO_3$ (Aldrich, <100 nm, 99.5%) bought from Aldrich and denoted as $SrTiO_3$-A was introduced as reference catalyst without further treatment.

A series of Au/$SrTiO_3$ photocatalysts with different loadings (0.49–3.0%) were prepared with deposition–precipitation method by using urea ($CO(NH_2)_2$, Wako, min. 99.0%) as the precipitating base, which permits the gradual and homogeneous addition of hydroxide ions throughout the whole solution. In general, 1.0 g of $SrTiO_3$ was added to 100 ml of an aqueous solution of $HAuCl_4$ (6.2×10^{-4} M, Wako, min. 99.0%) and urea (0.19 M). The suspension maintained at 80 °C was vigorously stirred for 4 h (pH increases), then centrifuged, washed, dried, and calcined at 400 °C for 4 h.

For comparison, Au/TiO_2 prepared with a similar procedure as Au/$SrTiO_3$ using Degussa P25 (Aldrich, 99.5%), TiO_2 with a diameter of 5 μm (Wako, min. 99.9%) TiO_2 with diameter of 25 nm (Aldrich, nanopowder, <25 nm, 99.7%) and ST-01 (Ishihara Sangyo Co., min. 99.0%) as support were introduced, denoted as Au/TiO_2-P25, Au/TiO_2-5 μm, Au/TiO_2-25 nm and Au/TiO_2-ST01, respectively. Commercial WO_3 (Wako, 95%) was also introduced as a reference catalyst without further treatment.

1.0% Au/SiO_2 was prepared with an impregnation method followed by calcination at 400 °C for 4 h. After drying at 70 °C for 10 h, the powder was calcined at 400 °C for 4 h. Two IrO_2/$SrTiO_3$ samples were prepared with the impregnation method and deposition–precipitation method, respectively. Both of the methods use Na_2IrCl_6 $6H_2O$ (Aldrich, 99.9%) as the precursor and are calcined at 400 °C for 4 h after drying. Ag/$SrTiO_3$ was prepared by a photodeposition method under UV light. The amount of Ag was 240 μmol, corresponding to the maximum amount of O_2 obtained over Au/$SrTiO_3$ (60 μmol, for more details see Results and discussion), while the loading was monitored by determining the O_2 evolution. Ag_2O/$SrTiO_3$ (120 μmol Ag_2O) was prepared *via* a similar method; the powder was calcined at 400 °C for 4 h after washing and drying.

Sample characterization

High-resolution transmission electron microscopy (TEM) characterization was performed with a JEOL 2100F operated at 200 kV. Powder X-ray diffraction (XRD) patterns of the products were recorded on an X'Pert PRO diffractometer with Cu-Kα radiation. X-Ray photoelectron spectroscopy (XPS) experiments were performed with a Theta probe (Thermo Fisher) using monochromated Al Kα X-rays. Valence band electronic structures were measured by hard X-ray photoemission spectroscopy (HX-PES) at the undulator beamline BL15XU of SPring-8. The photon energy was set to 5.95 keV. Sample powder was first dispersed in alcohol in air and dropped onto a carbon substrate. The sample was thoroughly dried in air and transferred into an ultra-high-vacuum (UHV) chamber attached to a high-resolution hemispherical electron spectrometer (VG Scienta R4000). The binding energy of photoelectrons was referenced to the Fermi energy of an Au film that was electrically contacted to the sample. The Brunauer–Emmett–Teller (BET) surface areas were measured *via* nitrogen physisorption (Gemini-2360; Micromeretics Corp., USA). Thermogravimetric (TG) and differential thermoanalysis (DTA) data were obtained on a Shimadzu DTG-60H DTA-TG apparatus under air flow with a heating rate of 10 °C min^{-1}. UV-vis diffusion reflectance absorption spectra

were recorded with a Shimadzu UV-2600, where an integrating sphere was used in diffusion reflectance absorption analysis.

Activity evaluation

Photocatalytic O_2 evolution was carried out with 0.2 g of photocatalyst suspended in 270 ml water in the presence of 5 mmol $AgNO_3$ (Wako, min. 99.8%) as a sacrificial reagent. A 300 W Xe arc lamp was employed as the light source. For visible-light ($\lambda >$ 400 nm) reaction, a L42 cutoff filter was used to remove UV light. The corresponding spectra of light source with and without filter are shown in Fig. S3.† As can be seen, the spectrum starts from 415 nm after adding the L42 cutoff filter. The concentrations of O_2 were detected by a gas chromatograph (GC-8A with TCD, Shimadzu).

Apparent quantum efficiencies at various wavelengths were measured by inserting a water filter and various band-pass filters in front of the reaction cell to obtain the desired incident wavelength. 430.0 nm, 480.4 nm, 518.7 nm, 549.3 nm, 617.7 nm and 660.0 nm band-pass filters (Optical Coatings Japan) were used to obtain the desired wavelengths, and the corresponding spectra were shown in Fig. S4.† For each wavelength region, the irradiation lasted for 14 h. The light intensities in the photocatalytic reaction were measured using a spectroradiometer (USR-40; Ushio Inc., Japan). Apparent quantum efficiency was obtained from the percentage of the number of reacted electrons during O_2 evolution and the number of incident photons.

Theoretical simulation

The absorption spectrum of Au NPs was simulated based on the Mie theory. The dielectric constant for Au was taken from Johnson and Christy's report.[38] A reflection index of 1.33 was used because Au NPs are mainly enclosed by water molecules under the reaction conditions. The nanoparticle diameter of 3 nm in simulation was obtained from the TEM average diameter data. In absorption spectra of Au NPs, an overlap of the SPR band and interband transition absorption edges was observed. After clarifying the contribution of the LSPR, the interband transition spectrum was obtained.

Results and discussion

Structure and morphology

A TEM image of $SrTiO_3$ (Fig. 1a) shows that the particle size of the as-prepared $SrTiO_3$ is around 20 nm. Meanwhile, $SrTiO_3$ (110) crystal planes can be easily discerned from a high resolution TEM image and confirmed by the corresponding fast Fourier transform patterns (inset, Fig. 1b), suggesting good crystallinity of $SrTiO_3$. The TEM images of 1.1% $Au/SrTiO_3$ shown in Fig. 1c and d indicate that Au NPs are highly dispersed with a mean particle size of 3 nm as suggested by the corresponding size distribution histogram (inset). In addition, distinct Au (200) crystal planes can also be observed in the HRTEM image. XRD patterns were also recorded for $SrTiO_3$ and $Au/SrTiO_3$ samples with different loadings (Fig. S5†). Characteristic $SrTiO_3$ diffraction peaks can be easily discerned from XRD patterns, and the average crystal size of $SrTiO_3$ was 25 nm

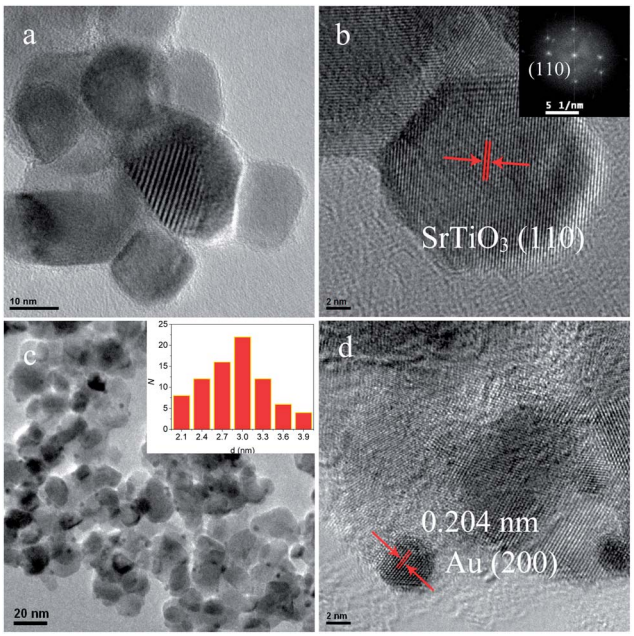

Fig. 1 TEM and HRTEM images of $SrTiO_3$ (a and b) and 1.1% $Au/SrTiO_3$ photocatalyst (c and d). Inset: fast Fourier transform patterns in image (b); distribution histogram corresponding to image (c).

as calculated from the most intensive (110) peak based on the Scherrer formula, which basically agrees with the results obtained from TEM images. In addition, the Au diffraction plane (200) with 2θ at 44.38° can be recognized over 1.1% and 3.0% $Au/SrTiO_3$. $Au/SrTiO_3$ photocatalysts were also characterized by conventional techniques in material sciences. N_2 adsorption measurements provided a specific surface area of 60.8 $m^2\ g^{-1}$ for 1.1% $Au/SrTiO_3$ (Fig. S6†). XPS analysis indicated that the chemical state of surface Au species in $Au/SrTiO_3$ was metallic Au after being calcined at 400 °C, while titanium in 4^+ and strontium in 2^+ state were also suggested (Fig. S7†).

Photophysical and photocatalytic properties

UV-vis diffusion reflectance spectra are shown in Fig. S8,† and the bandgap energy of $SrTiO_3$ is estimated with a Tauc plot, as shown in the figure inset. According to the Tauc plot, pure $SrTiO_3$ possesses a bandgap of 3.22 eV, *i.e.*, charge carriers (electrons and holes) in $SrTiO_3$ that can only be excited by UV light. A visible-light absorption, composed of strong absorption in the 400–500 nm range and an obvious LSPR peak centered at about 550 nm, is obtained after introducing Au NPs. The inhomogeneous broadening of plasmonic absorption observed in these measurements can be attributed to the inhomogeneity of the surrounding $SrTiO_3$ NPs and nanoparticle size distribution.[28]

O_2 evolutions under UV-visible irradiation were carried out (Fig. 2a), and 60.2 μmol O_2 was obtained over $SrTiO_3$ after being irradiated for 4 h. This is an expected result as charge carriers possessing sufficient redox potential can be excited in $SrTiO_3$ under UV irradiation. Furthermore, this activity is higher than that of the commercial $SrTiO_3$-A nanopowder (<100 nm)

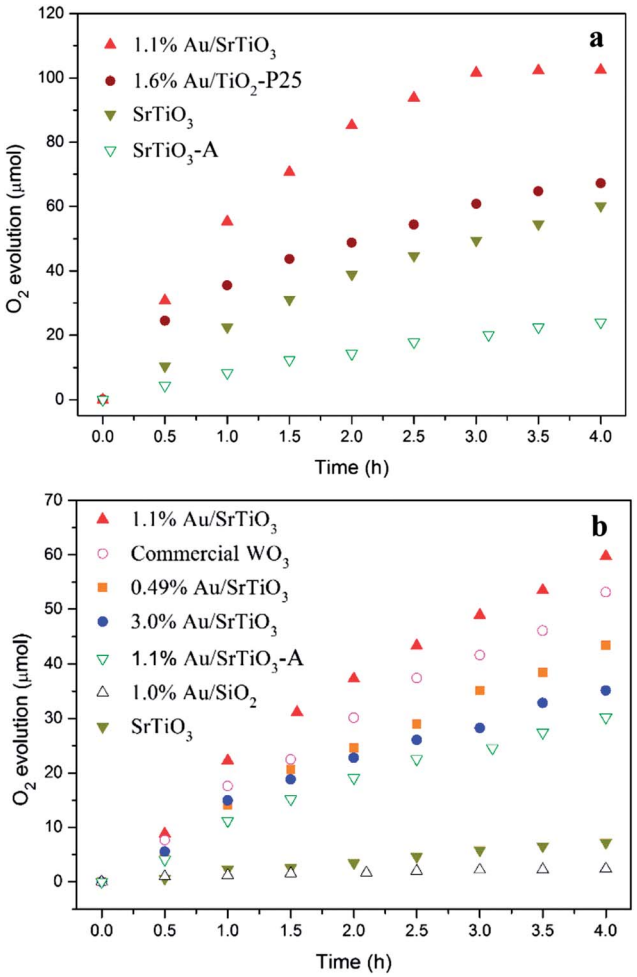

Fig. 2 (a) Curves of O_2 evolution as a function of reaction time under UV-visible light irradiation ($\lambda > 300$ nm); (b) curves of O_2 evolution as a function of reaction time under visible light irradiation ($\lambda > 400$ nm). Reaction conditions: 0.2 g catalyst, 5 mmol $AgNO_3$, 300 W Xe lamp.

purchased from Aldrich, which might be caused by higher crystallinity and finer crystal benefiting from the PC method, as suggested elsewhere.[29] The activity was enhanced by up to 0.7 times after Au NPs were introduced, indicating that the cocatalyst effect of Au in $Au/SrTiO_3$ for O_2 evolution is limited even when plasmonic enhancement is not taken into account. On the other hand, O_2 evolution activity, although lower than that of $Au/SrTiO_3$, was also obtained over Au/TiO_2 under UV-visible light as reported earlier.[18]

Subsequently, photocatalytic water oxidation under visible light was carried out (Fig. 2b). As expected, pure $SrTiO_3$ showed negligible activity as charge carriers in $SrTiO_3$ cannot be excited by visible light photons. A slight increase in activity after 2 h might be caused by Ag deposition.[30] It is remarkable that 43.4 μmol O_2 was obtained over 0.49% $Au/SrTiO_3$ after being irradiated for 4 h, suggesting that a visible-light photocatalytic activity was achieved by introducing Au NPs onto $SrTiO_3$. A slight increase of Au loading gives a positive effect on O_2 evolution activity. Specifically, 59.7 μmol O_2 in 4 h, *i.e.*, an average O_2 evolution rate of 14.9 μmol h^{-1}, was obtained over 1.1% $Au/SrTiO_3$. Furthermore, no obvious O_2 evolution rate loss was observed in 4 h, suggesting a relatively high durability of $Au/SrTiO_3$. O_2 evolution activity becomes lower when further increasing the gold loading to 3.0%, and a decrease of O_2 evolution rate along with reaction time was also observed. Although, the detrimental effect along with Au loading increase was also observed elsewhere,[31,32] the reason is not clear at this stage.[33] Inferior O_2 evolution activity was also obtained over $Au/SrTiO_3$-A, which is in accordance with the results under UV light.

In order to confirm that the observed visible-light activity is derived from $Au/SrTiO_3$ instead of interferences, a series of comparative experiments were carried out. First, Au NPs loaded on insulator SiO_2 were subjected to water oxidation under visible irradiation (Fig. 2b). Unlike $Au/SrTiO_3$, no O_2 evolution was obtained over Au/SiO_2, indicating a "synergistic effect" of $SrTiO_3$ and Au NPs in the composite photocatalyst rather than solely accounting for the visible-light water oxidation activity. IrO_2 is a well-known O_2 evolution cocatalyst which is much more efficient than Au.[34] In order to eliminate the cocatalyst effect in $Au/SrTiO_3$, IrO_2 loaded $SrTiO_3$ prepared with different methods was also evaluated (Fig. 3a). Negligible O_2 evolution was obtained over $IrO_2/SrTiO_3$ prepared with deposition–precipitation method, while only a slight increase was observed when the impregnation method was adopted, indicating that the visible-light activity obtained over $Au/SrTiO_3$ should be induced by the photosensitization of Au NPs instead of a cocatalyst effect. Because Ag also possesses a plasmonic effect and a gradual deposition of Ag occurs during the O_2 evolution, evaluation over $Ag/SrTiO_3$ prepared with the photodeposition method was also carried out. As can be seen from Fig. 3a, negligible activity was observed even when the maximum amount of Ag was loaded at the initial stage. However, 13.3 μmol O_2 was obtained in 4 h over $Ag_2O/SrTiO_3$, indicating Ag_2O as a semiconductor can be involved in water oxidation. However, the rate is much less than that of $Au/SrTiO_3$ (59.7 μmol O_2 in 4 h). Furthermore, reduction from Ag^+ with electrons and immersion in water might make silver mainly stay in the metal state, which has a negligible contribution. Therefore, the contribution of Ag_2O in water oxidation over $Au/SrTiO_3$ in this work is limited. Based on these results, we could draw a conclusion that the observed visible-light O_2 evolution activity should mainly be induced by the $Au/SrTiO_3$ composite. Moreover, 1.1% $Au/SrTiO_3$ was also subjected to H_2 evolution under visible irradiation (Fig. 3a). The results showed that 47.8 μmol H_2 was obtained in 4 h; further discussion of this result will be provided in the mechanism part of the study.

As Au NP photosensitization over TiO_2 has been reported for visible-light water oxidation,[18] four Au/TiO_2 samples varying in TiO_2 phase and particle size were also employed for comparison (Fig. 3b). Among them, Au/TiO_2 in which Degussa P25 served as a support, showed superior activity; *i.e.*, 12.2 μmol O_2 was obtained after being irradiated for 4 h, which basically agrees with an early report.[18] Superior activity over Au photosensitized P25 should be caused by the presence of an anatase and rutile TiO_2 heterojunction effect. Commercial WO_3 as a reference photocatalyst was also subjected to water oxidation under

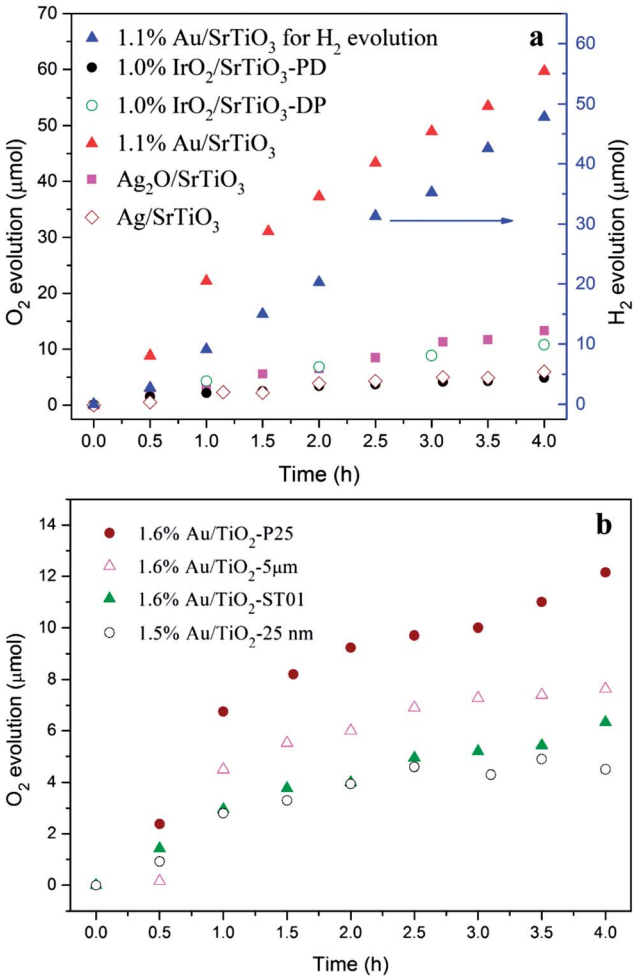

Fig. 3 Curves of O_2 or H_2 evolution as a function of reaction time under visible light irradiation (λ > 400 nm) (a and b). Reaction conditions: 0.2 g catalyst, 300 W Xe lamp, 5 mmol $AgNO_3$ for O_2 evolution; 0.2 g catalyst (0.5 wt% Pt), 300 W Xe lamp, 50 ml methanol for H_2 evolution.

visible light, and 53.1 μmol O_2 was obtained in 4 h (Fig. 2b). It is worth pointing out that the O_2 evolution activity over $Au/SrTiO_3$ is about 4.9 times as much as that of Au/TiO_2 and even slightly higher than that of the commercial WO_3 evaluated under the same conditions. In other words, $Au/SrTiO_3$ is a promising candidate for water oxidation under visible light.

Mechanism study

The underlying mechanism of Au NP photosensitization over a semiconductor remains elusive, although some potential physical pathways have been put forth, among which LSPR mediated direct electron transfer from plasmonic metal to semiconductor and separation of charge carriers in semiconductor induced by LSPR energy transfer are the most popular ones.[9] In order to gain insight into the gold photosensitization process in $Au/SrTiO_3$ during visible-light water oxidation, an elaborate study was carried out from three perspectives: electron transfer, driving force, and relative band positions in $Au/SrTiO_3$.

Clarifying electron transfer direction

In the composite $Au/SrTiO_3$ nanostructure, charge carrier transfer under visible light might occur, while the direction will be different depending on the site where the separation of charge carriers takes place (in $SrTiO_3$ or Au NPs). Water oxidation in the presence of $AgNO_3$ as a sacrificial regent offers a good opportunity to clarify the electron transfer direction in $Au/SrTiO_3$ through studying the Ag location after the reaction. If photo-excited electrons in Au transfer to $SrTiO_3$, Ag^+ will be mainly reduced on $SrTiO_3$ surface, as illustrated in Fig. 4a. On the contrary, when charge carrier separation takes place in $SrTiO_3$, Ag^+ will be mainly reduced on Au as electrons excited in $SrTiO_3$ accumulate on Au due to its large work function, as shown in Fig. 4b.[35] Then 1.1% $Au/SrTiO_3$ after being irradiated with visible light (λ > 440 nm) for 1 h in the presence of $AgNO_3$ was subjected to a HAADF-STEM and EDS study. In the HAADF-STEM image shown in Fig. 5a, bright spots, Au, Ag or both of them can be discerned from the background. Apart from particle 2 having a size of about 8 nm, the sizes of the other three particles range from 15 to 30 nm. As Au NPs in $Au/SrTiO_3$ possess a mean size of about 3 nm, those metal particles should mainly or completely be composed of Ag. The compositions of particles 1 and 2 were first studied with EDS spot scanning (Fig. 5b). Pure Ag composition of particle 1 with a diameter of 27 nm was apparent, while Au core with Ag shell (approximately 4 nm in thickness) nanostructure can be discerned in particle 2. Elemental mapping results further confirmed the composition of particles 1 and 2, and revealed that particles 3 and 4 were also pure Ag (Fig. 5c–f). Some random sole spots should be caused by interferences from other elements. That is, Ag^+ reductions by electrons mainly occur on the surface of $SrTiO_3$, indicating that the photo-excited electron transfer from gold to $SrTiO_3$ should be dominant in this system. This result agrees well with the observed visible-light H_2 evolution activity over $Au/SrTiO_3$.

Au interband transition driven by hot electron transfer

With the purpose of figuring out the source of electrons transferred from gold to $SrTiO_3$ or the driving force for water oxidation, a theoretical simulation study on Au NP's optical excitation was first carried out based on Mie theory (Fig. 6). The simulated absorption is very similar to the UV-vis absorption of prepared

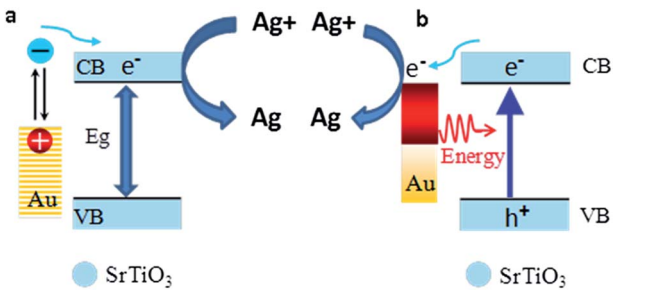

Fig. 4 Illustration of the Ag^+ reduction in different processes: electrons transfer from Au to $SrTiO_3$, (a); charge carrier separation in $SrTiO_3$, (b).

Au NPs with a mean diameter of about 3 nm, indicating that the simulation model is well established. After subtracting the contribution of the LSPR,[36] an obvious interband transition of Au NPs tailing to about 520 nm was obtained, which is attributed to d–sp transition.[37] This result agrees with that suggested by Johnson and Christy,[38] in which the first interband excitation of Au occurs at the X-point in the Brillouin zone, at an energy of 2.5 eV.

An apparent quantum efficiency (AQE) study, which is usually used to ascertain the real driving force in photocatalysis, was carried out over 1.1% Au/$SrTiO_3$ for water oxidation (Fig. 6). The standard deviations are less than 0.78×10^{-2}%, indicating good measurement reproducibility. Impressively, AQE decreases along with the increase in wavelength, though this trend is slightly mitigated around 530 nm, which is obviously different from the Au NP LSPR spectrum obtained in both the experiments and the simulation. This result gives clear evidence that Au NP photosensitization over $SrTiO_3$ for water oxidation under visible light is not, at least not primarily, driven by an LSPR related electromagnetic field or electron collective oscillations, because they are all closely related to their excitation wavelength. On the other hand, the main part of the AQE curve with high values bears strong resemblance to the interband transition band, indicating that hot electrons transferred from Au mainly arise from these interband transitions. This assumption is also supported by the negligible O_2 evolution over Ag/$SrTiO_3$ under visible irradiation because the interband transitions of Ag are only excited in the ultraviolet spectrum though the plasmon resonance and can be observed in the visible region.[39] The decreasing trend of AQE is slightly mitigated around 530 nm and tails up to 660 nm, which might be caused by the LSPR nonradiative decay *via* interband and intraband excitations.[40] It should be pointed out that photodecomposition of organic pollutant (*e.g.*, iso-propanol in our previous work[10]) or aerobic oxidation is not necessarily driven by interband transitions as even near-infrared light photons have sufficient energy to drive plasmonic electron transfer from metal to semiconductor where they can activate O_2 to intermediates (O_2^- and/or H_2O_2), which can be involved in further oxidation.[41,42]

Relative band position in Au/$SrTiO_3$

In order to clarify the oxidative potential of the leaving holes on Au in the interband transition, the valence band (VB) maximum of $SrTiO_3$ as well as the band edge of Au nanopowders were measured (Fig. 7a). The VB maximum of $SrTiO_3$ lies at 3.20 eV, which is inconsistent with an early report.[43] Because the band gap of $SrTiO_3$ is 3.22 eV from optical absorption spectrum, the E_F is rather close to its conduction band (CB) minimum. For Au nanopowders, a 5d-band edge lies at 1.95 eV relative to its E_F, while the lower part tailing up to E_F is attributed to 6sp electrons.[44] Alignment of Fermi levels of $SrTiO_3$ and Au NPs will occur after contact and will be equilibrated again after irradiation. As hot electrons transfer from Au NP to CB of $SrTiO_3$ under visible light, this accumulation of electrons on the semiconductor would cause a negative shift (relative to NHE) of the aligned E_F.[45] Therefore, in this study, the aligned E_F in Au/$SrTiO_3$ after equilibration under visible light irradiation is assumed to be located at the original E_F of $SrTiO_3$. By taking account of the CB minimum of $SrTiO_3$ lying around −0.3 V *vs.* NHE and a slight band bending after contact (*ca.* 0.3 eV),[46,47] a schematic illustration of Au/$SrTiO_3$ band energy can be obtained, Fig. 7b. As can be seen, the leaving holes on Au have a potential of *ca.* 1.67 V *vs.* NHE, which is located well below the potential of water oxidation (1.23 V *versus* NHE).[48] Meanwhile, the minimum energy required for valence electrons from Au to flow onto $SrTiO_3$ CB is 2.27 eV, corresponding to 546 nm photons, which is larger than the threshold of gold interband transition (520 nm) from simulation. That is, from both energy and relative band position, electrons from interband transitions in gold have sufficient energy to transfer into the CB of $SrTiO_3$, while the leaving holes possessing enough oxidative potential should be responsible for water oxidation, which agrees well with the results obtained from the electron transfer and driving force study.

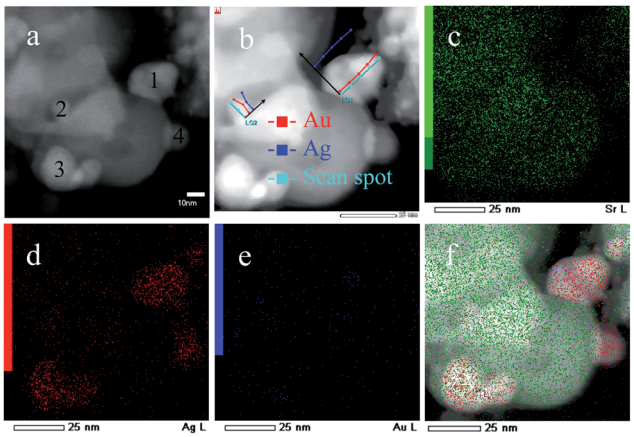

Fig. 5 HAADF-STEM image (a), EDS spot scans (b) and EDS mapping (c–f) of the Au/$SrTiO_3$ after being irradiated with visible light (λ > 440) for 1 hour in the presence of $AgNO_3$ as sacrificial reagent.

Since it was first proposed by Tatsuma's group, LSPR induced direct electron transfer from a metal to a semiconductor was frequently cited to explain the enhanced visible-light photocatalytic performance obtained over plasmonic catalysts.[49,50] It finds experimental support where an increase of the photocurrent matches exactly with the wavelength distribution of the LSPR band in photoelectrocatalysis.[51] However, such improvements in photocurrent have also been explained by changes in light scattering or reflection,[52] and a recent study also suggests the intensity of electron transfer and is not necessarily correlated with an Au LSPR band.[27,53] Furthermore, considering that plasmonic electrons reside around the Fermi level of the metal, plasmonic charge carriers are proposed to be insufficient in energy to drive harsh oxidation requiring high oxidative potentials.[17] A comparison of the potentials of holes created in Au LSPR and interband transitions was theoretically studied by Govorov and co-workers.[54] Their results suggest that photo-generated holes in the interband transition are created far from the Fermi surface (2.4 eV relative to E_F), while holes in

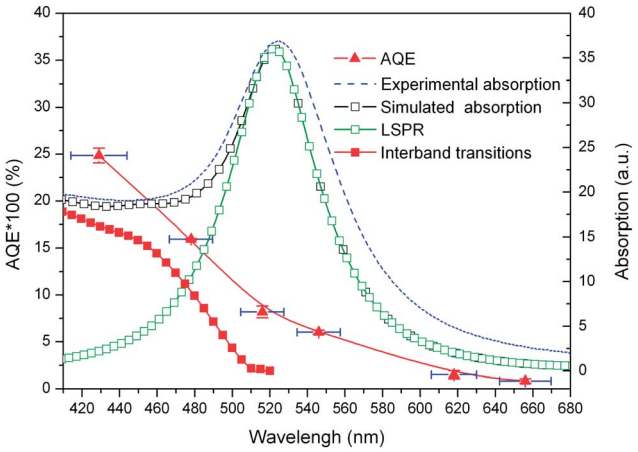

Fig. 6 Apparent quantum efficiencies (AQE) of O_2 evolution over 1.1% $Au/SrTiO_3$ at various light wavelength; UV-vis absorption of Au NPs with a mean diameter of about 3 nm; simulated absorption of Au NPs with a diameter of 3 nm, consisting of SPR and interband transition. Vertical error bars correspond to the standard deviation of AQE, while horizontal error bars represent the wavelength range.

the plasmonic wave are distributed near the Fermi surface. These results agree well with the Au photosensitization process revealed in this work that gold interband transitions are the main driving force in visible-light water oxidation over $Au/SrTiO_3$, though LSPR related decay through interband transition might also contribute to this process. As pointed out in the results and discussion, $Au/SrTiO_3$ exhibits a superior visible-light O_2 evolution activity as compared with Au/TiO_2. However, it is difficult to give a clear explanation at this stage because the underlying mechanism of Au NPs in the Au/TiO_2 system is still elusive despite numerous efforts.[7] One possible reason lies in the more negative (relative to NHE) conduction band of $SrTiO_3$ as compared with TiO_2, which facilitates Ag^+ reduction with electrons transferred from Au, and ultimately enhances the water oxidation activity. Similar phenomena have also been reported in our previous work and elsewhere.[55,56]

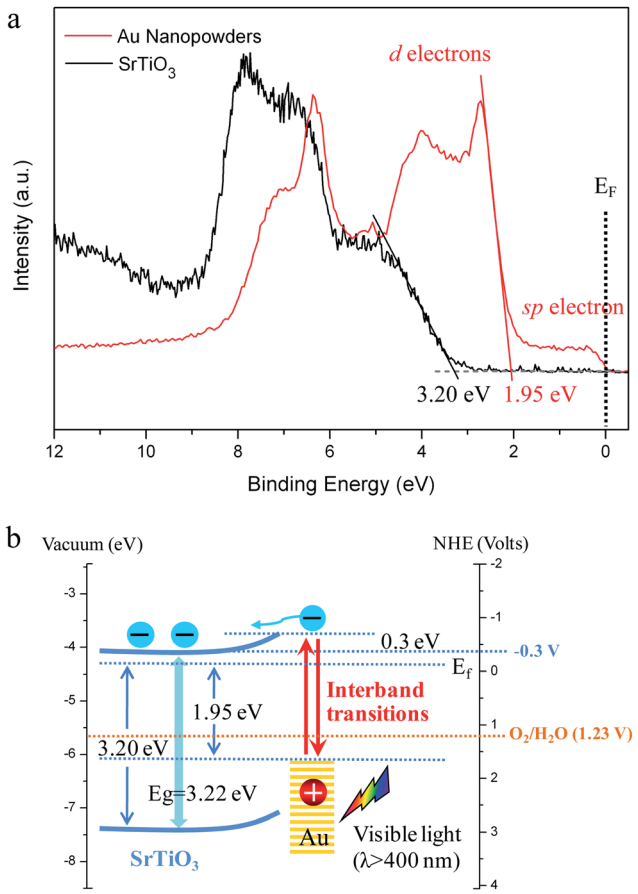

Fig. 7 (a) Valence band XPS spectrum of $SrTiO_3$ and band edge Au nanopowders; (b) schematic illustration of energy band position in $Au/SrTiO_3$ composite nanostructure.

Conclusions

In summary, a remarkable visible-light photocatalytic water oxidation activity was achieved over Au NP photosensitized $SrTiO_3$, which offers a promising visible-light responsive candidate for photocatalytic water oxidation. Direct electron transfer from gold to $SrTiO_3$ in photosensitization is confirmed by STEM-EDS study on selective Ag deposition over $SrTiO_3$ during water oxidation. An Au interband transition driven direct electron transfer photosensitization process is revealed based on AQE results, a theoretical simulation study on Au NP optical excitation and the relative band position analysis in $Au/SrTiO_3$, *i.e.*, hot electrons transferred from gold to $SrTiO_3$ in visible-light water oxidation mainly come from Au interband transitions, while leaving holes are responsible for water oxidation. The capability of involving Au interband transition in photosensitization for visible-light water oxidation not only provides an alternative explanation for the photosensitization role of Au NPs, but also opens up new opportunities in designing and preparing visible-light responsive photocatalysts.

Acknowledgements

This work received financial support from the World Premier International Research Center Initiative (WPI Initiative) on Materials Nanoarchitectonics (MANA), the National Basic Research Program of China (973 Program, 2014CB239301) and the JST PRESTO program from the Ministry of Education, Culture, Sports, Science and Technology (MEXT).

References

1 H. Tong, S. Ouyang, Y. Bi, N. Umezawa, M. Oshikiri and J. Ye, *Adv. Mater.*, 2012, **24**, 229–251.
2 A. Fujishima and K. Honda, *Nature*, 1972, **238**, 37–38.
3 X. B. Chen, L. Liu, P. Y. Yu and S. S. Mao, *Science*, 2011, **331**, 746–750.
4 R. Konta, T. Ishii, H. Kato and A. Kudo, *J. Phys. Chem. B*, 2004, **108**, 8992–8995.
5 D. F. Wang, J. H. Ye, T. Kako and T. Kimura, *J. Phys. Chem. B*, 2006, **110**, 15824–15830.
6 P. Wang, B. Huang, Y. Dai and M. H. Whangbo, *Phys. Chem. Chem. Phys.*, 2012, **14**, 9813–9825.

7 W. Hou and S. B. Cronin, *Adv. Funct. Mater.*, 2013, **23**, 1612–1619.
8 S. C. Warren and E. Thimsen, *Energy Environ. Sci.*, 2012, **5**, 5133.
9 S. Linic, P. Christopher and D. B. Ingram, *Nat. Mater.*, 2011, **10**, 911–921.
10 L. Liu, S. Ouyang and J. Ye, *Angew. Chem., Int. Ed.*, 2013, **52**, 6689–6693.
11 M. Xiao, R. Jiang, F. Wang, C. Fang, J. Wang and J. C. Yu, *J. Mater. Chem. A*, 2013, **1**, 5790.
12 S. Linic, P. Christopher, H. Xin and A. Marimuthu, *Acc. Chem. Res.*, 2013, **46**, 1890–1899.
13 H. M. Chen, C. K. Chen, C.-J. Chen, L.-C. Cheng, P. C. Wu, B. H. Cheng, Y. Z. Ho, M. L. Tseng, Y.-Y. Hsu, T.-S. Chan, J.-F. Lee, R.-S. Liu and D. P. Tsai, *ACS Nano*, 2012, **6**, 7362–7372.
14 P. A. Desario, J. J. Pietron, D. E. Devantier, T. H. Brintlinger, R. M. Stroud and D. R. Rolison, *Nanoscale*, 2013, **5**, 8073–8083.
15 Y. Nishijima, K. Ueno, Y. Kotake, K. Murakoshi, H. Inoue and H. Misawa, *J. Phys. Chem. Lett.*, 2012, **3**, 1248–1252.
16 Z. W. Liu, W. B. Hou, P. Pavaskar, M. Aykol and S. B. Cronin, *Nano Lett.*, 2011, **11**, 1111–1116.
17 A. Primo, T. Marino, A. Corma, R. Molinari and H. Garcia, *J. Am. Chem. Soc.*, 2011, **133**, 6930–6933.
18 C. G. Silva, R. Juarez, T. Marino, R. Molinari and H. Garcia, *J. Am. Chem. Soc.*, 2011, **133**, 595–602.
19 S. N. Habisreutinger, L. Schmidt-Mende and J. K. Stolarczyk, *Angew. Chem., Int. Ed.*, 2013, **52**, 7372–7408.
20 A. Kudo and Y. Miseki, *Chem. Soc. Rev.*, 2009, **38**, 253–278.
21 G. V. Hartland, *Chem. Rev.*, 2011, **111**, 3858–3887.
22 S. Naya, A. Inoue and H. Tada, *ChemPhysChem*, 2011, **12**, 2719–2723.
23 H. Zhu, X. Ke, X. Yang, S. Sarina and H. Liu, *Angew. Chem.,Int. Ed.*, 2010, **49**, 9657–9661.
24 W. B. Hou, W. H. Hung, P. Pavaskar, A. Goeppert, M. Aykol and S. B. Cronin, *ACS Catal.*, 2011, **1**, 929–936.
25 H. Zhu, X. Chen, Z. Zheng, X. Ke, E. Jaatinen, J. Zhao, C. Guo, T. Xie and D. Wang, *Chem. Commun.*, 2009, 7524–7526, DOI: 10.1039/b917052a.
26 A. Furube, L. Du, K. Hara, R. Katoh and M. Tachiya, *J. Am. Chem. Soc.*, 2007, **129**, 14852–14853.
27 J. B. Priebe, M. Karnahl, H. Junge, M. Beller, D. Hollmann and A. Bruckner, *Angew. Chem., Int. Ed.*, 2013, **52**, 11420–11424.
28 S. Mukherjee, F. Libisch, N. Large, O. Neumann, L. V. Brown, J. Cheng, J. B. Lassiter, E. A. Carter, P. Nordlander and N. J. Halas, *Nano Lett.*, 2013, **13**, 240–247.
29 Y. Miseki, H. Kato and A. Kudo, *Energy Environ. Sci.*, 2009, **2**, 306–314.
30 D. B. Ingram, P. Christopher, J. L. Bauer and S. Linic, *ACS Catal.*, 2011, **1**, 1441–1447.
31 K. Kimura, S.-i. Naya, Y. Jin-nouchi and H. Tada, *J. Phys. Chem. C*, 2012, **116**, 7111–7117.
32 G. R. Bamwenda, S. Tsubota, T. Nakamura and M. Haruta, *J. Photochem. Photobiol., A*, 1995, **89**, 177–189.
33 A. Primo, A. Corma and H. Garcia, *Phys. Chem. Chem. Phys.*, 2011, **13**, 886–910.
34 J. Ran, J. Zhang, J. Yu, M. Jaroniec and S. Z. Qiao, *Chem. Soc. Rev.*, 2014, DOI: 10.1039/c3cs60425j.
35 G. Hansson and S. Flodström, *Phys. Rev. B: Condens. Matter Mater. Phys.*, 1978, **18**, 1572–1585.
36 M. A. Garcia, *J. Phys. D: Appl. Phys.*, 2011, **44**, 283001.
37 R. C. Jin, *Nanoscale*, 2010, **2**, 343–362.
38 P. B. Johnson and R. W. Christy, *Phys. Rev. B: Solid State*, 1972, **6**, 4370–4379.
39 J. S. Sekhon and S. S. Verma, *Plasmonics*, 2012, **7**, 453–459.
40 C. Sonnichsen, T. Franzl, T. Wilk, G. von Plessen, J. Feldmann, O. Wilson and P. Mulvaney, *Phys. Rev. Lett.*, 2002, **88**, 077402.
41 E. Kowalska, R. Abe and B. Ohtani, *Chem. Commun.*, 2009, 241–243, DOI: 10.1039/b815679d.
42 Y. Sugano, Y. Shiraishi, D. Tsukamoto, S. Ichikawa, S. Tanaka and T. Hirai, *Angew. Chem., Int. Ed.*, 2013, **52**, 5295–5299.
43 S. A. Chambers, T. Droubay, T. C. Kaspar and M. Gutowski, *J. Vac. Sci. Technol., B: Microelectron. Nanometer Struct.–Process., Meas., Phenom.*, 2004, **22**, 2205.
44 M. G. Ramchandani, *J. Phys. C: Solid State Phys.*, 1970, **3**, S1–S9.
45 V. Subramanian, E. E. Wolf and P. V. Kamat, *J. Am. Chem. Soc.*, 2004, **126**, 4943–4950.
46 N. Serpone and E. Pelizzetti, *Photocatalysis:Fundamentals and Applications*, Wiely, New York, 1989.
47 K. Mitsuhara, Y. Kitsudo, H. Matsumoto, A. Visikovskiy, M. Takizawa, T. Nishimura, T. Akita and Y. Kido, *Surf. Sci.*, 2010, **604**, 548–554.
48 S. Mubeen, J. Lee, N. Singh, S. Kramer, G. D. Stucky and M. Moskovits, *Nat. Nanotechnol.*, 2013, **8**, 247–251.
49 Y. Tian and T. Tatsuma, *Chem. Commun.*, 2004, 1810–1811, DOI: 10.1039/b405061d.
50 Y. Tian and T. Tatsuma, *J. Am. Chem. Soc.*, 2005, **127**, 7632–7637.
51 Z. Zhang, L. Zhang, M. N. Hedhili, H. Zhang and P. Wang, *Nano Lett.*, 2013, **13**, 14–20.
52 R. Solarska, A. Krolikowska and J. Augustynski, *Angew. Chem., Int. Ed.*, 2010, **49**, 7980–7983.
53 L. Du, A. Furube, K. Hara, R. Katoh and M. Tachiya, *J. Photochem. Photobiol., C*, 2013, **15**, 21–30.
54 A. O. Govorov, H. Zhang and Y. K. Gun'ko, *J. Phys. Chem. C*, 2013, **117**, 16616–16631.
55 R. Niishiro, S. Tanaka and A. Kudo, *Appl. Catal., B*, 2014, **150–151**, 187–196.
56 S. X. Ouyang and J. H. Ye, *J. Am. Chem. Soc.*, 2011, **133**, 7757–7763.

